ELSEVIER

Catalysis Today 50 (1999) 651–660

CATALYSIS TODAY

Application of integrated computational chemistry system to the design of inorganic membranes

Hiromitsu Takaba, Koichi Mizukami, Yasunori Oumi, Momoji Kubo, Abhijit Chatterjee, Adil Fahmi, Akira Miyamoto*

Department of Materials Chemistry, Graduate School of Engineering, Tohoku University, Aobayama-07, Aramaki, Aoba-ku, Sendai, 980-8579, Japan

Abstract

Today inorganic membranes attract a lot of interest as a growing field. Main focus of those activities is on the development of membrane materials, which can offer high permselectivities with acceptable high permeances. The need for high permselectivity beyond those limited by Knudsen flow requires the estimation of the factors, which determine the permselectivity. Plausible theoretical models based on physical or chemical reasoning is desirable to guide systematic development efforts for designing next generation inorganic membranes. Here we reviewed our attempts to generate theoretical models based on the molecular dynamics method for this purpose. As a first attempt, simulation was performed at specific conditions where the Knudsen theory can be applied and can be reproduced well by our simulation methodology. Molecular dynamics simulation at 373 K of the permeation of iso- and *n*-butanes through ZSM-5 type silicalite membrane are presented. After 200 ps of simulation time the permeation of *n*-butane was observed whereas the permeation of iso-butane was not observed. The calculated permeability of *n*-butane, which is close to experimental data, is also presented. A study on the affinity membrane for the separation of CO_2 at high temperature is presented and the prospect of permselectivity of CO_2 is demonstrated.

Keywords: Knudsen flow; Inorganic membranes; Molecular dynamics

1. Introduction

Porous and dense inorganic membranes have been investigated extensively as the possible gas separation medium. In particular, porous membranes (e.g. ceramic and zeolite membranes) exhibit high permeabilities relative to dense membranes and thermal and chemical stabilities relative to organic membranes [1,2]. In order to design a high performance membrane, the assessment of transport mechanism of gases is needed, as the transport mechanism is the fundamental of the characterization of selectivity and permeability of membranes. The transport mechanism, however, depends on various properties, such as the intrinsic properties of the molecules, the membrane structure, the affinity of the molecule towards the membrane and physical conditions (temperature, pressure, etc.). Thus, the separation mechanism in a microporous membrane is not yet well understood.

*Corresponding author. Address: Faculty of Engineering, Department of Molecular Chemistry and Engineering, Tohoku University, Sendai, 980-77, Japan. Tel.: +81-2-217-7233; fax: +81-2-217-7235; e-mail: miyamoto@aki.che.tohoku.ac.jp

0920-5861/99/$ – see front matter
PII: S0920-5861(98)00499-4

For example, the experimental permeance studies of iso- and *n*-butanes through zeolite membranes show that, in general, *n*-butane has a higher permeance than iso-butane [3–6]. However, some studies [7] have shown that iso-butane permeability becomes larger than that of *n*-butane at high temperatures. Such a temperature dependency implies the complexity of the transport mechanism.

Molecular dynamics (MD) allows the description of the dynamic behavior of the transport mechanism. As to our knowledge, few studies have applied this method to inorganic membrane system. In this paper, we present the results of MD studies on the inorganic membrane systems namely Knudsen flow on ceramic membrane, butane isomer permeation on the zeolite membrane and CO_2 separation on the affinity membrane. Attempts made to characterize the dynamics of gas permeation on the inorganic membranes at molecular level are reviewed.

2. Computational methodology

We used a modified MXDORTO program [8] for MD calculations. Our modifications are relative to the temperature control and the many body potential describing hydrocarbons. The temperature was controlled by scaling atomic velocities under three-dimensional periodic boundary conditions. The temperature of the gas phase is separately scaled from that of the membrane in order to set the gas temperature at the desired value when the temperature of the gas is significantly lower or higher than the desired value. The Verlet algorithm was used for the calculation of atomic motions, while the Ewald method was used to calculate the electrostatic interactions. For any pair of atoms labeled as i and j in the unit cell, their interaction potential is given by the following expression:

$$U_{ij} = Z_i Z_j e^2/r_{ij} + f_0(b_i + b_j)\,\exp[(a_i + a_j - r_{ij})/(b_i + b_j)] + 4\epsilon_{ij}\{(\sigma_{ij}/r_{ij})^{12} - (\sigma_{ij}/r_{ij})^{6}\} + V. \quad (1)$$

The first three terms refer to Coulomb, exchange-repulsion, and Lennard-Jones (LJ) potentials, respectively. Z is the atomic charge, e the elementary electric charge, r_{ij} (Å) the interatomic distance, and f_0 ($=6.9511\times10^{-11}$ N) is a constant for unit adaptations. The parameters a and b in the exchange-repulsion potential represent the size and the stiffness of the atoms, respectively. ϵ_{ij} and σ_{ij} characterize the LJ potential. The second term (exchange-repulsion) is applied only to atoms of the membrane, whereas the third term is used to describe the interaction between nonbonded species; i.e. gas–gas and gas–membrane interactions. The fourth term, V, is the many body potential which describes the bonding within the butane molecule:

$$V = D_b[1 - \exp[-a(b - b_0)]]^2 + h_\theta(\theta - \theta_0)^2 + h_\phi\{1 + \cos(n\phi - \phi_0)\}. \quad (2)$$

These terms refer to the bond stretching, b, the angle bending, θ, and the torsion angle, ϕ, and D_b, a, h, and n are constants. All the potential parameters used are given in [9–11]. They are based on the parameters obtained from the consistent valence force field (CVFF) developed by Hagler et al. [12,13]. For the visualization of the interacting system during the simulation, we used the real time solid modeling RYUGA program [14].

3. Theoretical studies of permeation based on Knudsen flow

For gas transport in micropores (less than 1 nm), the contribution of viscous flow can be neglected and Knudsen flow becomes the most fundamental transport mechanism. In this section, we present the studies on the simulation of Knudsen flow using NVT ensemble MD (the numbers of particles, volume and temperature are constant.) [11]. We estimated gas permeability and compared with the existent theoretical value from Knudsen theory.

We performed our calculations at a condition where the Knudsen diffusion mechanism is followed. Here we considered He and Ar as gas atoms. Knudsen factor in our model is 0.94 and 0.71 for He and Ar, respectively. The permeability of the system governed by the Knudsen flow, is given by [11]:

$$q = 4/3 \times pr(2RT/\pi M)^{1/2}(n_1/V_1 - n_2/V_2)/d, \quad (3)$$

where d is the membrane thickness, p the porosity, V the volume and n is the number of molecules. Subscripts 1 and 2 indicate the gas and the vacuum

phase, respectively. The permeability appears as a linear function of the number of molecules. However, MD calculations give the number of permeated molecules as a function of time $n(t)$. Therefore, we interpolate $n(t)$ assuming a parabolic function ($a{\cdot}t^2+b{\cdot}t+c$), the derivative dn/dt corresponds to the permeability.

We employed MgO ceramic membrane model with a thickness of 15 Å and a cylindrical pore placed at the center of the membrane has a diameter of 11 Å. Another poreless MgO membrane (bulkhead membrane) of a thickness of 2 Å is added to the bottom of the unit cell to prevent the periodic diffusion. The pressure difference between the two phases divided by the membrane (namely the gas phase and the vacuum phase) is the driving force for the permeation. The membrane is expected to move down under the pressure during the simulation, to prevent this displacement, we fixed two layers from the bottom of the membrane.

3.1. He and Ar permeation

We placed 128 Helium atoms above the membrane to examine Helium permeability and to investigate its permeating behavior. The temperature was kept at 773 K. The interaction of gas towards MgO bulkhead membrane is presented by LJ potential, which includes two fitting parameters. The energy parameter in the LJ potential between He gas and atoms in the membrane (Mg and O) is 100 K (=0.1 kcal/mol), which is very weak compared with the kinetic energy of gas intended to attain the condition of Knudsen flow. The affinity of the gas towards the membrane was maintained as very weak (ϵ_{ij}=0.20 kcal/mol for He atoms in membrane) in order to attain the condition of the Knudsen flow. Fig. 1 represents the computer graphics (CG) images of the He permeation through membrane after 0.625, 23.125, and 50 ps. The Helium gas flows directly through the pore without any adsorption on the membrane. Fig. 2 shows the correlation between our MD permeabilities and those obtained from the Knudsen equation (3). They are in good agreement which means that the Knudsen flow is reproduced well by this simulation method.

We also investigated the permeation rate for a mixture of He–Ar gas (He=64 atoms, Ar=64 atoms) following the same procedure. The affinity of Ar and

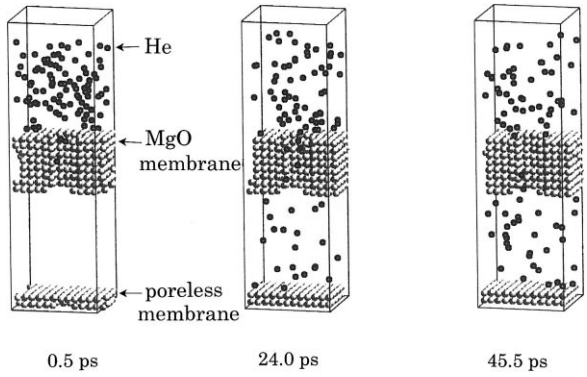

Fig. 1. He permeation through the MgO membrane at 773 K. Only half of MD unit cells are shown.

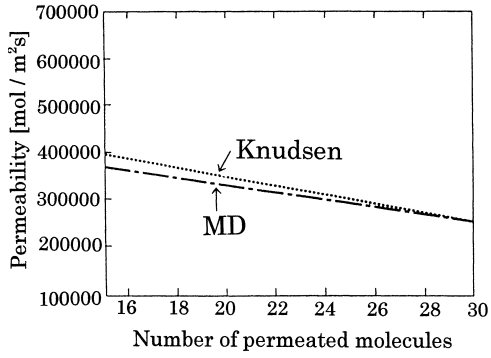

Fig. 2. He permeability through the MgO membrane at 773 K.

He towards the membrane was also kept very weak (ϵ_{ij}=0.20 kcal/mol). The permeability depends mainly on the molecular weight and therefore the light species are expected to permeate faster. Fig. 3 represents the time evaluation of the separation factor, which is defined as the ratio of number of permeated atoms (He/Ar) into the vacuum phase, with the estimated value by Knudsen flow. Since we can clearly see a good agreement between these two values, Knudsen flow of mixture of gas is also reproduced well. The separation factor decreases with the increase in the simulation time and this behavior can be explained as follows. In the beginning of simulation He atoms permeate faster and therefore He concentration decreases in the gas phase whereas Ar concentration increases, which decreases the separation factor with time.

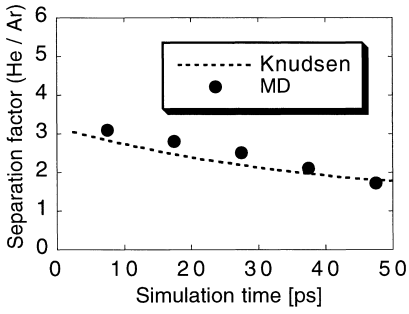

Fig. 3. The time evaluation of the separation factor for the mixed He–Ar gas at 773 K: closed circle is MD simulation and dashed line is Knudsen theory results.

4. Theoretical studies of permeation based on other flow mechanisms

The separation factor in Knudsen flow is defined as the inverse of the root of molecular mass. Thus, for the separation of molecules having similar mass, other transport mechanisms are required to achieve the higher separation factor. Molecular sieving and the interactions of gas molecules with the membrane are possible alternatives and can enhance the separation factor.

In this section, we present the MD studies on the gas permeation capabilities of zeolite and affinity membranes. The results show that the permeation process based on molecular sieving or the interactions of gas molecules with the membrane occurs.

4.1. Separation of butane isomers on MFI type zeolite membrane

Zeolite membrane has gained much attention as novel membrane materials. We report here the studies on the permeation of butane isomers through the ZSM-5 type silicalite membrane [10].

The geometry of the silicalite membrane model was taken from the available X-ray diffraction data [15]. We employed the *Pnma* orthorhombic structure with cell parameters, a=20.02 Å, b=19.99 Å, and c=13.38 Å. One unit cell of ZSM-5 contains two straight channels, two sinusoidal channels, and two channel intersections. The membrane has a (0 1 0) external surface. Hydrogen atoms were added to unsaturated surface oxygen atoms which lead to the formation of surface silanol groups. Fig. 4 shows the different projections of the membrane model.

The arrangement of silanol groups on the surface was obtained by relaxing the system at 300 K. The model consists of a unit cell with three-dimensional periodic boundary conditions and a thickness of 14.0 Å, the total number of atoms is 256. A fixed

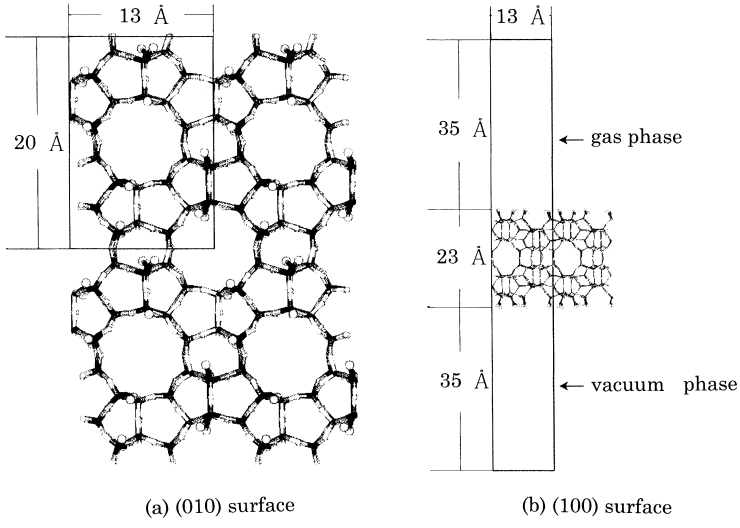

Fig. 4. Model of a ZSM-5 type silicalite membrane used in the present study: (a) top view of the membrane surface (0 1 0) and (b) side view (1 0 0).

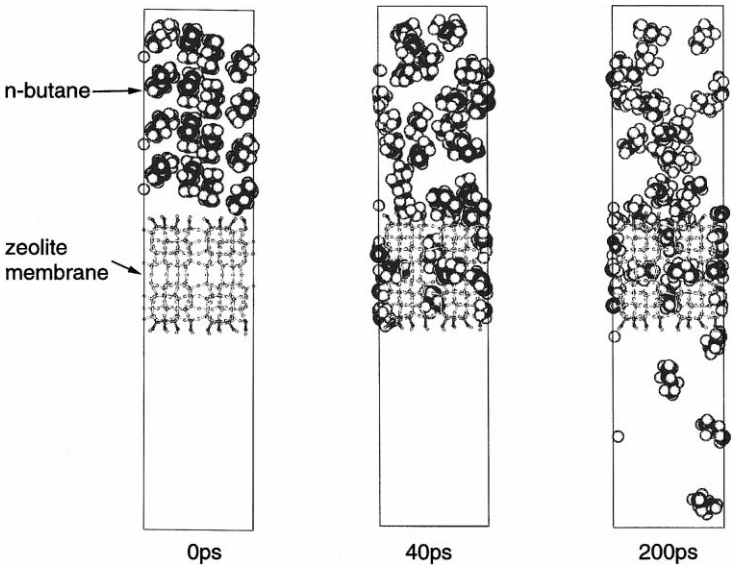

Fig. 5. Permeation of *n*-butane gas through a silicalite membrane at 373 K.

wall was constructed to prevent the periodic diffusion of the molecules along the z direction and the molecules can therefore reflect on this wall. The geometry of surface hydroxyl groups and Si atoms in membrane were fixed in order to maintain the structure, whereas O atoms of the zeolite framework were relaxed.

4.1.1. Permeation dynamics of n-butane through the MFI membrane

Fig. 5 shows the MD calculation results of *n*-butane single gas diffusion through the membrane at 373 K. Initially, 16 *n*-butane molecules were arranged in four layers in the gas phase. This configuration was relaxed using molecular mechanics (before performing MD calculation) to avoid the rapid increment of the temperature of atoms caused by their arbitrary geometries. This minimization procedure was applied for all initial states. *n*-Butane diffused into both straight and sinusoidal channels. After 40 ps, all allowed spaces for adsorption in the zeolite channels were saturated, but yet no molecule was permeating. At 86 ps, the permeation through the silicalite membrane was started. Since the permeation starts only after the saturation of the membrane, the diffusion mechanism is then a capillary condensation or surface diffusion. This is in agreement with previous experimental observation which reported the condensation of *n*-butane inside the silicalite pore at the time of permeation [4–7]. Fig. 6 shows the permeation dynamics of *n*-butane through the silicalite membrane at 773 K. At 10 ps, the molecules were diffusing into the straight and sinusoidal channels and finally reached the outlet of the straight channel. The observed diffusion speed through the channels is significantly faster than that at 373 K. At 147 ps, some molecules have already permeated into the vacuum phase, and the membrane pores were not saturated. At 773 K, the adsorption effect appeared to be relative by less. The kinetic energy of a butane molecule in the gas phase at 773 K is 2.3 times larger than that at 373 K. This increase in the kinetic energy leads to the permeation without condensation.

In order to analyze the effect of the temperature on the adsorption, the amount of adsorbed species in silicalite pore per ps time at 373 and 773 K were determined and the results are shown in Fig. 7. At 373 K, the amount of *n*-butane increases rapidly with time and then reaches a constant value indicating that the transport mechanism is governed by the interaction of molecules with pore wall. At 773 K, the amount of *n*-butane is smaller than that at 373 K. This reveals that the contribution of the interaction of molecules with pore wall becomes less when the temperature is increased.

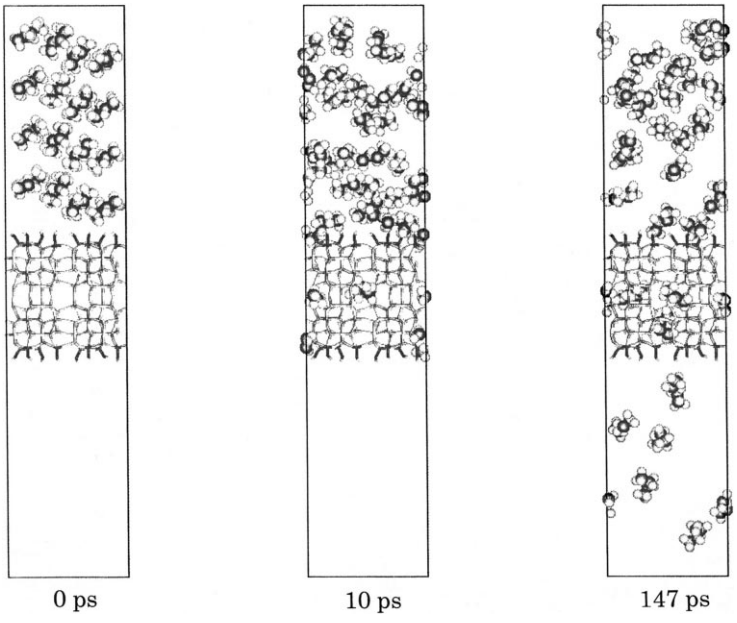

Fig. 6. Permeation of *n*-butane gas through a silicalite membrane at 773 K.

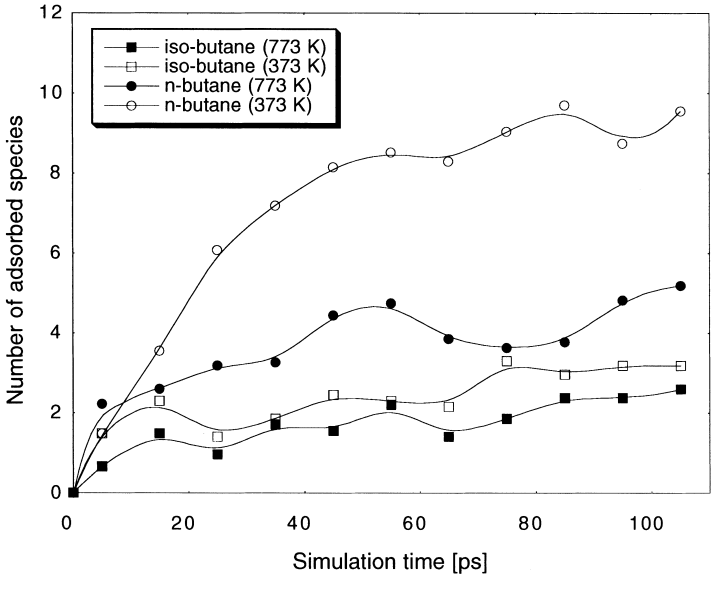

Fig. 7. The amounts of adsorbed iso- and *n*-butane in the silicalite pore at 373 and 773 K obtained from MD calculations.

4.1.2. Permeation dynamics of iso-butane through the MFI membrane

Fig. 8 shows the MD simulation results of iso-butane single gas permeation at 373 K. After 250 ps of simulation no permeation was observed, except the diffusion of some molecules are diffusing into the straight channel. This indicates that the permeance of iso-butane is significantly smaller than that of *n*-butane. Experimentally the permeance of iso-butane is at least one order of magnitude smaller than that of

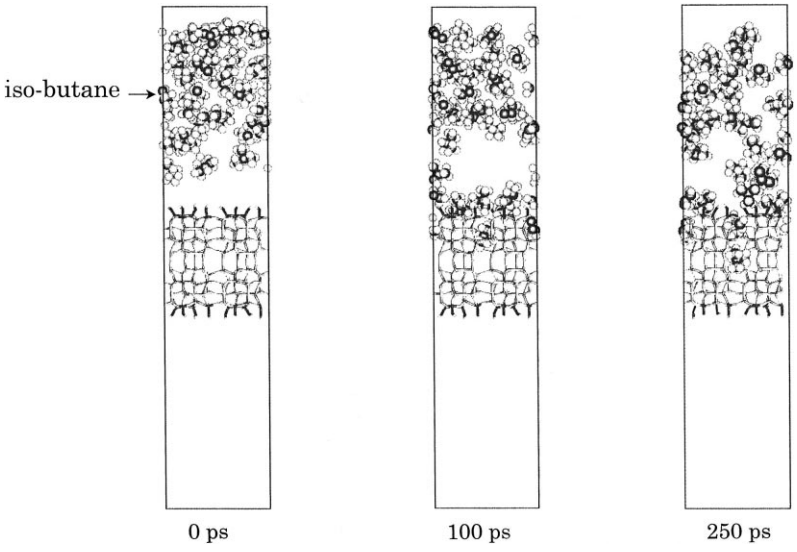

Fig. 8. Diffusion of iso-butane through a silicalite membrane at 373 K.

n-butane [4,6]. From the real time visualization, we observed the aggregation of iso-butane molecules around the entrance of the straight channel. This is due to the molecular size which is close to the pore diameter. Therefore, most of the molecules collide with the pore wall which decreases their velocity and enhances their condensation around the entrance of the pore. Molecules that are succeeded to enter the straight channel diffuse into the intersection between sinusoidal and straight channels, and go back to the gas phase. We performed further MD simulation at higher temperature, 773 K. Even at this temperature, the permeation of iso-butane was not observed after 250 ps of simulation. However, the diffusion into the sinusoidal channel was observed. Therefore, at high temperature iso-butane can diffuse in all channels of the silicalite. The amount of adsorbed iso-butane shown in Fig. 7 is smaller than *n*-butane, and even the effect of the temperature seems less important. It seems that the steric hindrance of iso-butane around the pore entrance affects the diffusion dynamics into the pore.

4.1.3. Permeability analysis

We calculated the permeability of *n*-butane single gas from the results of MD calculation. Fig. 9 shows the time evolution of permeated molecules of *n*-butane

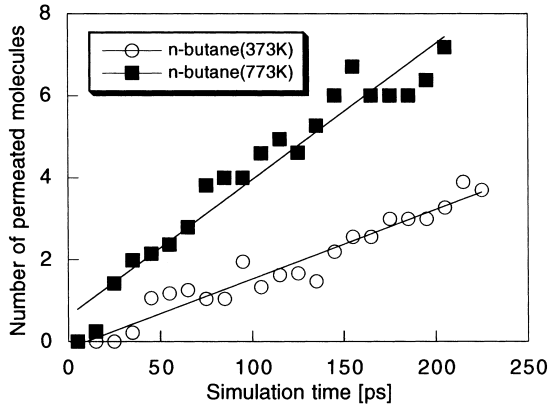

Fig. 9. The time evaluation of permeated *n*-butane molecules at 373 and 773 K obtained from the MD calculation of single gas system.

at 373 and 773 K. The permeance at 773 K is approximately two times the value at 373 K. The plotted curves are proportional to the simulation time. Since the permeance is function of pressure, in case of Knudsen flow it is expected to decrease with the increase of simulation time since the gas pressure (difference between gas and vacuum phase pressures) will decrease with permeation. Thus, this result reveals that the other flow mechanism is dominant

Table 1
Calculated and experimental permeabilities of *n*-butane

Reference	Permeability (mol m/m^2 s Pa)	Temperature (K)	Membrane thickness
[5]	4.5×10^{-12}	298	50 μm
[6]	1.18×10^{-12}	298	5 μm
[16]	0.80×10^{-12}	300	40 μm
This study	1.4×10^{-12}	373	23 Å

in the permeation of *n*-butane in comparison to Knudsen flow. Table 1 represents the calculated permeability of *n*-butane at 373 K together with the available experimental data. The permeability Q is given by $Q=D\times L/(S\times P)$, where D is the derivative relative to time of the permeated molecules, L the membrane thickness 23 Å, S the surface area of the membrane per unit cell facing the gas phase 280.4 Å^2, and P is the gas pressure. The gas pressure is given by the equation of state of perfect gases, with a gas volume of 9814 Å^3. We calculated the pressure as 162 atm at 373 K. Table 1 shows that our calculated value is close to the available experimental data. The sketched experimental permeabilities are in a wide range, because the permeability is sensitive to the structure of the membrane and in particular to the presence of the crack.

4.2. Affinity membrane for CO_2 separation

The affinity of gas molecules with the membrane can be used for the direct separation of CO_2 at high temperature (>800°C) from the exhaust gas, which is almost released from all typical stationary sources such as thermal power plants or fossil flue combustion in large factories [17,18]. In this section, we present the MD studies on the effect of affinity for the CO_2 separation from CO_2/N_2 mixture gas [9].

Affinity strength in this simulation is represented by the following interatomic potential:

$$(r_{ij}) = 4u_{ij}\{(r^*_{ij}/r_{ij})^6 - (r^*_{ij}/r_{ij})^{12}\},$$

where u_{ij} (kcal/mol) is the affinity strength and r_{ij}^* (Å) is the interatomic distance. MgO solid with slit-like pore having a diameter of 6.3 Å was used as the membrane model (See Fig. 10). The real affinity of MgO crystal for CO_2 and N_2 are not considered and we simulated different affinity models in order to examine the effect of affinity for separation behavior. Both CO_2 and N_2 molecules are treated as a single sphere model in order to perform simulations for a reasonable long time. All calculations were done at 1073 K because we focused on the high temperature process.

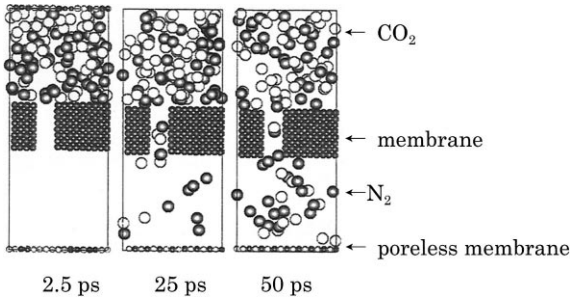

Fig. 10. The dynamic behavior of the model representing a weak affinity between the CO_2 molecule and the wall of membrane, the affinity of CO_2 and N_2 to the wall of membrane were 0.2 kcal/mol. Light sphere molecules represent CO_2, dark ones N_2.

4.2.1. Dynamics behavior of weak affinity model

In Fig. 10, we show the snap shots representing the results of our simulation of diffusion of CO_2 and N_2. This model represents a weak affinity model, where the affinity of CO_2 and N_2 molecule for the wall of membrane atom were 0.2 kcal/mol ($=u_{ij}$). It can be seen that both CO_2 and N_2 diffused through the membrane to vacuum phase with increment in time steps. Fig. 11 shows the change of number of molecules in the vacuum phase with increment in time steps. It is indicated that N_2 has more diffusivity compared to CO_2, and selective CO_2 separation is impossible. The number of permeated molecules in the vacuum phase increased logarithmically in the beginning of the steps and it became almost constant at 70 ps. It follows from this result that after 70 ps the driven force of the permeation from the gas phase to

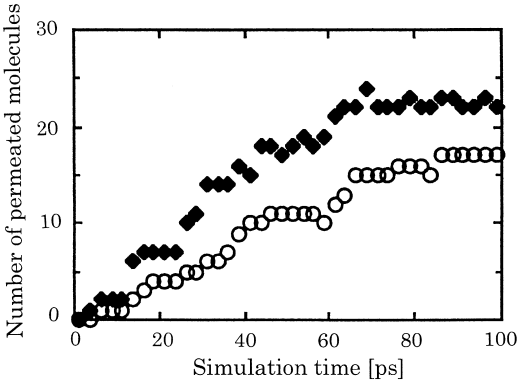

Fig. 11. The change of number of permeated molecules as time step increment, in a weak affinity model. Open circle represents CO_2 and closed diagram corresponds to N_2.

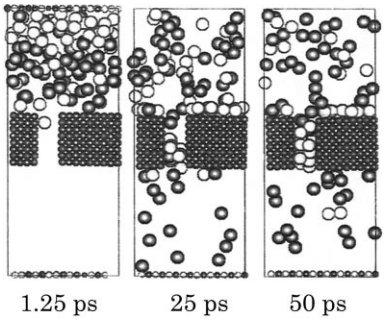

Fig. 12. The dynamic behavior of the model representing a strong affinity between the CO_2 molecule and the wall of membrane, the affinity of CO_2/N_2 to the wall of membrane were 1.2 and 0.2 kcal/mol, respectively.

the vacuum phase become very moderate due to the decrease in pressure difference between both phases and the two phases reached equilibrium state. One of the interesting observations is that the numbers of permeated molecules for both gases are different, although the initial ratio of CO_2/N_2 in the gas phase was equal. Separation factor for the CO_2/N_2 molecules in the vacuum phase from the result of beginning of this calculation is about 0.76 which is in good agreement with separation factor of 0.8 expected by Knudsen diffusion mechanism. Thus, we can conclude that Knudsen diffusion mechanism dominates the separation behavior in this system.

4.2.2. Dynamics behavior of strong affinity model

Fig. 12 shows the result of the model representing a strong affinity between the CO_2 molecule and the membrane. The affinity of CO_2 and N_2 for the membrane were 1.2 and 0.2 kcal/mol, respectively. It is observed that both molecules could diffuse to the vacuum phase in the beginning of the simulation, however, with increasing the simulation time, CO_2 molecules were captured in the micropore and preferably condensed in the micropore. Selective condensation behavior is characteristic of the affinity membrane.

Further dynamics behavior was investigated. We used the configuration shown in Fig. 12 at 50 ps as initial configuration for the current study. The number of molecules in the gas phase was replaced by the initial situation where CO_2: N_2 is 1.0, and the gas molecules in the vacuum phase which have already permeated after the 50 ps run were also removed. This procedure represents the simulation of the process in which the membrane pore has been already filled with permeable gas molecules. This situation can be seen in actual continuous membrane processes. Fig. 13 shows the results of the simulation. At any time step, CO_2 molecules are preferred to condense in the micropore and it seems to block the diffusion of N_2 into the micropore. Fig. 14 shows the change of the number of CO_2 and N_2 molecules in the vacuum phase. Selective CO_2 permeation is indicated, while the permeation of N_2 is suppressed. This figure indicates that the affinity membrane is useful for the separation of CO_2 from CO_2/N_2 mixture gas at high temperature.

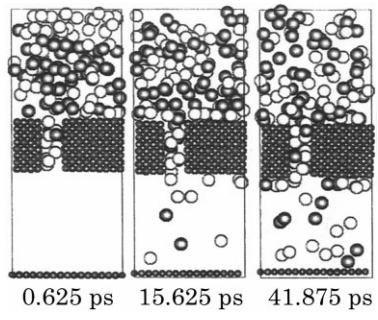

Fig. 13. The dynamic behavior of the model representing a strong affinity model. Initial configuration is taken from the result in Fig. 12 at 50 ps. See contents for details.

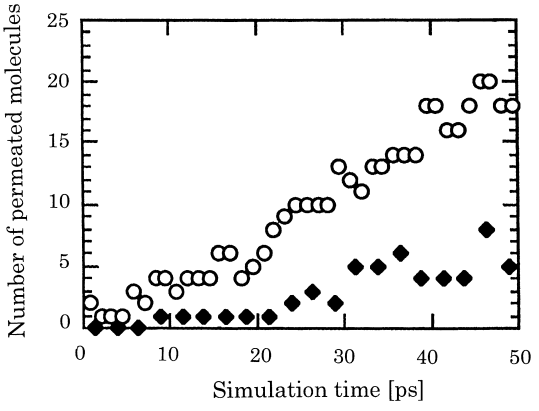

Fig. 14. The changes of number of permeated molecules in the vacuum phase as time steps increasing, in a strong affinity model. Open circle refers to CO_2 and closed diagram to N_2.

5. Conclusions

We reviewed our molecular dynamics studies on the gas permeation through the inorganic membrane. The Knudsen flow on the MgO model membrane and other flow on the silicalite membrane were demonstrated. The results are in good agreement with experimental results. The prospect of CO_2 separation at 1073 K using the affinity membrane was presented. The contents of the above reports can be summarized to conclude that the computational studies have an impact on inorganic membranes at present and will be a strong useful methodology for designing the novel effective inorganic membranes in the near future. In this paper, it has only been possible to highlight a few studies using molecular dynamics simulations. There are various methodologies for molecular simulation, e.g. Monte Carlo simulation, virtual reality system for material design, quantum calculation or first principle molecular dynamics, etc. They can be substantially applicable to any other problems of inorganic membranes. Moreover, with the advance of computing power, more accurate molecular simulations will become feasible in the foreseeable future.

References

[1] H.P. Hsieh, Inorganic Membranes for Separation and Reaction, Elsevier, Amsterdam, 1996.
[2] A.J. Burggraaf, L. Cot, Fundamentals of Inorganic Membrane Science and Technology, Elsevier, Amsterdam, 1996.
[3] K. Kusakabe, S. Yoneshige, A. Murata, S. Morooka, J. Membr. Sci. 116 (1996) 39.
[4] M.-D. Jia, B. Chen, R.D. Noble, J.L. Falconer, J. Membr. Sci. 90 (1994) 1.
[5] E.R. Geus, H. van Bekkum, W.J.W. Bakker, J.A. Moulijin, Micropor. Mater. 1 (1993) 131.
[6] C. Bai, M.-D. Jia, J.L. Falconer, R.D. Noble, J. Membr. Sci. 105 (1995) 79.
[7] Z.A.E.P. Vroon, K. Keizer, M.J. Gilde, H. Verweij, A.J. Burggraaf, J. Membr. Sci. 113 (1996) 293.
[8] K. Kawamura, in: F. Yonezawa (Ed.), Molecular Dynamics Simulations, Springer, Berlin, 1992, p. 88.
[9] H. Takaba, K. Mizukami, M. Kubo, A. Stirling, A. Miyamoto, J. Membr. Sci. 121 (1996) 251.
[10] H. Takaba, R. Koshita, K. Mizukami, N. Ito, M. Kubo, A. Fahmi, A. Miyamoto, J. Membr. Sci. 134 (1997) 127.
[11] K. Mizukami, H. Takaba, M. Kubo, A. Fahmi, A. Miyamoto, Appl. Surf. Sci. 119 (1997) 330.
[12] A.T. Hagler, S. Lifson, P. Dauber, J. Am. Chem. Soc. 101 (1979) 5122.
[13] J.-R. Hill, J. Sauer, J. Phys. Chem. 98 (1994) 1238.
[14] R. Miura, H. Yamano, R. Yamauchi, M. Kubo, A. Miyamoto, Catal. Today 23 (1995) 409.
[15] D.H. Olson, G.T. Kokotailo, S.L. Lawton, W.M. Meier, J. Chem. Phys. 85 (1981) 2238.
[16] F. Kapteijin, W.J.W. Bakker, J. van de Graaf, G. Zheng, J. Poppe, J.A. Moulijin, Catal. Today 25 (1995) 213.
[17] T. Suda, M. Fuji, K. Yoshida, M. Iijima, T. Seto, S. Mitsuoka, Energy Convers. Mgmt. 33 (1992) 317.
[18] M.J. Cogbill, G.P. Marsh, Energy Convers. Mgmt. 33 (1992) 487.